

Physical and spectroscopic properties of pure C₂H₄ and CH₄:C₂H₄ ices

Germán Molpeceres,¹ Miguel Angel Satorre,² Juan Ortigoso,¹ Alexandre Zanchet,³ Ramón Luna,² Carlos Millán,² Rafael Escribano,¹ Isabel Tanarro,¹ Víctor J. Herrero¹ and Belén Mate^{1*}

¹Instituto de Estructura de la Materia, IEM-CSIC, Serrano 121, E-28006 Madrid, Spain

²Centro de Tecnologías Físicas, Universitat Politècnica de València, EPSA, E-03801 Alcoy, Spain

³Instituto de Física Fundamental, IFF-CSIC, Serrano 123, E-28006 Madrid, Spain

Accepted 2016 December 2. Received 2016 November 18; in original form 2016 October 14

ABSTRACT

Physical and spectroscopic properties of ices of C₂H₄ and CH₄:C₂H₄ mixtures with 3:1, 1:1 and 1:3 ratios have been investigated at 30 K. Two laboratories are involved in this work. In one of them, the density and refractive index of the samples have been measured by using a cryogenic quartz microbalance and laser interferometric techniques. In the other one, IR spectra have been recorded in the near- and mid-infrared regions, and band shifts with respect to the pure species, band strengths of the main bands, and the optical constants in both regions have been determined. Previous data on ethylene and the mixtures studied here were scarce. For methane, both the wavenumbers and band strengths have been found to follow a regular pattern of decrease with increasing dilution, but no pattern has been detected for ethylene vibrations. The method employed for the preparation of the samples, by vapour deposition under vacuum, is thought to be adequate to mimic the structure of astrophysical ices. Possible astrophysical implications, especially by means of the optical constants reported here, have been discussed.

Key words: methods: laboratory: solid state – techniques: spectroscopic – catalogues – planets and satellites: composition – infrared: planetary systems.

1 INTRODUCTION

The results of the *New Horizons* mission recently published by Gladstone et al. (2016) show a great variability on the characteristics of the surface of Pluto in color, morphology or chemical composition. Pluto's surface has been known to contain N₂, CH₄ and CO, C₂H₆, C₂H₄ (Cruikshank et al. 2015; Merlin 2015 and references therein). *New Horizons* data reveal also the presence of old terrains with craters and processed ices, in contrast with other younger surfaces with relatively high albedo, characteristic of non-processed ices. The results provided by this mission open the possibility of the occurrence of CH₄ segregation from nitrogen as was previously suggested by Douté and collaborators (Douté et al. 1999). An indirect proof of this segregation could be the atmospheric composition. LORRI and Alice data (Gladstone et al. 2016) of the atmospheric profile of Pluto show N₂, CH₄ and also C₂H_x absorptions, the latter below 420 km. One of the most plausible explanations for the presence of C₂H_x in the atmosphere is that these molecules are formed by processing of a methane rich region on the surface. In order to obtain C₂H_x, methane ice should be segregated from the

other volatiles, as otherwise the products of irradiation would bear nitrogen or oxygen in their composition. The formation of C₂H_x hydrocarbons from irradiation of CH₄ ices is widely demonstrated in the laboratory (de Vries et al. 1984; Kaiser & Roessler 1992; Strazzulla et al. 2002).

Methane, and in some cases C₂H₆, has also been detected in other trans-Neptunian objects (TNOs) like Makemake, Sedna and Quaoar (see DeMeo et al. 2010; Barucci et al. 2010; Cruikshank et al. 2015).

All of this evidence suggests that studies of mixtures of CH₄ and C₂H₄, as those provided in this article, may be helpful for the comprehension of chemical composition and evolution of the ice surfaces of Pluto, but also of other outer Solar system bodies.

In the laboratory, methane ice has been thoroughly studied both pure and mixed with other gases (Hudgins et al. 1993; Mulas et al. 1998; Gálvez et al. 2009; Gerakines & Hudson 2015; Molpeceres et al. 2016). It is known that at 30 K it presents a rotationally disordered crystalline phase, and by deposition at 20 K or below a more ordered crystalline structure is formed. The literature about ethylene ice is not so large. Zhao and coworkers (Zhao, Ospina & Khanna 1988) gave mid infrared (IR) intensities and optical constants of crystalline C₂H₄ ice at 55 K. Near IR spectra of pure C₂H₄, or isolated in a nitrogen matrix, were investigated by Quirico

* E-mail: belen.mate@csic.es

and Schmitt (Quirico & Schmitt 1997), who obtained absorption coefficients for the pure species in the near IR. More recently, different solid phases of ethylene ice were investigated by Hudson and coworkers (Hudson, Gerakines & Moore 2014) in the near- and mid- IR, and the optical constants and band strengths for the different forms were provided. A crystalline phase was grown by these authors at 60 K, while by fast deposition at 20 K they found a different crystalline phase that was named metastable. In this latter work a careful revision of the spectroscopic data about ethylene ice available in the literature was conducted. Recently, some experiments of energetic processing of C_2H_4 diluted in N_2 ice have been reported (Chen et al. 2015), aimed to analyse the different reaction products that are formed when using the Lyman α radiation of hydrogen or 500 eV electrons as energetic processing agents. However, to the best of our knowledge, no results involving spectroscopic and physical properties of $CH_4:C_2H_4$ ice mixtures are available.

In this paper, we have undertaken an investigation of $CH_4:C_2H_4$ ice mixtures, as a continuation of our previous work on $CH_4:C_2H_6$ mixtures (Molpeceres et al. 2016). The temperature of the experiments has been chosen as a compromise between the certainty of no sublimation of methane in our experimental setups, and the relevance in an astronomical context. Since the planetary bodies for which our study can be relevant have a surface temperature ranging from 30 K of Makemake and Eris to around 40 K of Pluto, and since methane ice has a sublimation temperature of around 40 K in our experimental conditions, the experiments were performed at 30 K.

Our work is organized along three lines: first, the measurement of densities and visible refractive indices of C_2H_4 and $CH_4:C_2H_4$ ice mixtures; then, a study of spectra, band positions, band shifts (with respect to the pure species), and infrared band strengths of these ice mixtures at 30 K; finally, the optical constants in the near-infrared (NIR) and mid-infrared (MIR) regions. We describe also the experimental setups used in this work, and, at the end, we discuss some astrophysical implications and enumerate the conclusions.

2 EXPERIMENTAL SETUP

This work has been carried out in two different laboratories, one devoted to measurements of density and visible refractive index, and the other to IR spectroscopy of ices. They have been described elsewhere (Satorre et al. 2013; Zanchet et al. 2013; Molpeceres et al. 2016), so that only a brief description is given here.

The first laboratory is located in Alcoy. It consists of a high vacuum chamber provided with a quartz crystal microbalance in thermal contact with the cold head of a closed cycle helium cryostat. The microbalance measures the mass deposited on its sensible surface per square centimeter. In addition, a double interferometric He–Ne laser technique is used to measure the visible refractive index, n_0 , of the ice deposited on the microbalance and its thickness. Knowing the layer thickness and mass, the density of the ice is determined. Background deposition, backfilling the whole chamber with the gas of interest, is used in these experiments to ensure the formation of a uniform ice layer and an accurate measurement of the density. The film is formed at a constant rate of deposition by maintaining a constant pressure of the gases in a prechamber, and using a needle valve to connect it with the high vacuum chamber. Gases used in these experiments are CH_4 (99.999 5 per cent Praxair) and C_2H_4 (99.95 per cent Praxair). Most of the experiments are carried out at 2.0 nm s^{-1} ,

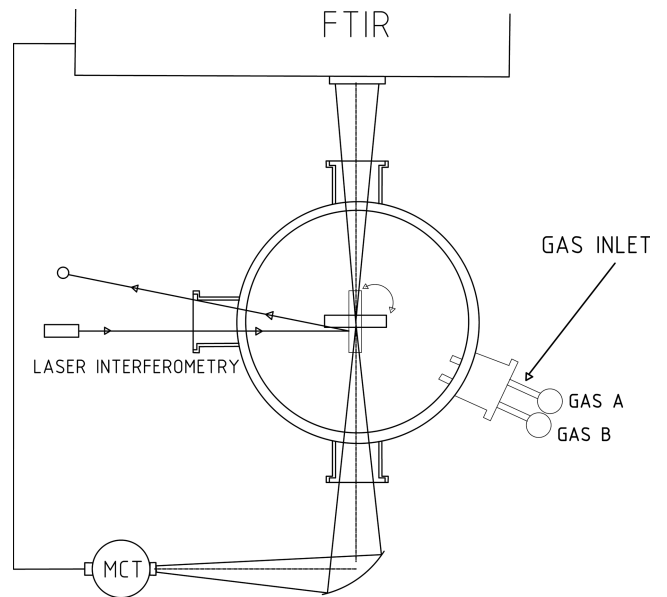


Figure 1. Scheme of the experimental setup for IR spectroscopy measurements.

but in a separate set of experiments deposition rates have been four times slower and faster, and no appreciable changes in the density and refractive index have been observed. Film thickness ranges from 1 to 2 microns. This technique is applied to ices of pure species and mixtures.

The IR spectroscopy laboratory is sited in Madrid and consists of a vacuum chamber that also works in the high vacuum regime (1×10^{-8} mbar) and is provided with a closed cycle helium cryostat. A Vertex 70 FTIR spectrometer is coupled to the chamber through KBr windows. Gases CH_4 (99.95 per cent Air Liquide) and C_2H_4 (99.5 per cent Air Liquide), are introduced into the chamber through independent lines equipped with mass flow controllers operating in the ranges between 2 and 10 sccm, backfilling the system to a desired pressure in the 10^{-6} mbar range. The gases condense on an IR transparent Si substrate (1 mm thick) that is in close contact with the cold finger of the cryostat, forming two ice layers of equal thickness on each side of the substrate. The gas inlet flange is situated in the vacuum chamber 10 cm below the end of the cold finger of the cryostat and directed to the chamber walls, to ensure that gas molecules fill the chamber with a homogeneous pressure and do not reach the cold substrate directly, but are rather deposited from the background gas forming a homogeneous ice layer. Deposition rates vary between 1.0 and 2.0 nm s^{-1} . Ice thickness is measured during deposition following the interference pattern of a He–Ne laser (628 nm) in quasi normal (4° angle) reflection configuration (see Fig. 1). Once the ice layer is grown the substrate is rotated to face the IR radiation, and normal incidence transmission spectra of the system ice/Si/ice are recorded in the NIR ($8000\text{--}3000 \text{ cm}^{-1}$) and MIR regions, using specific beam splitters and lamps for each spectral range but the same MCT detector. The set of spectroscopic properties derived in this work are extracted from ice layers of thickness up to ~ 6.5 or $\sim 1.4 \text{ }\mu\text{m}$ for NIR or MIR, respectively. Special attention was paid to avoid saturation of the strong absorption bands in the MIR spectra. Spectra were taken by co-adding 100 scans with 1 and 2 cm^{-1} resolution for the NIR and MIR regions, respectively.

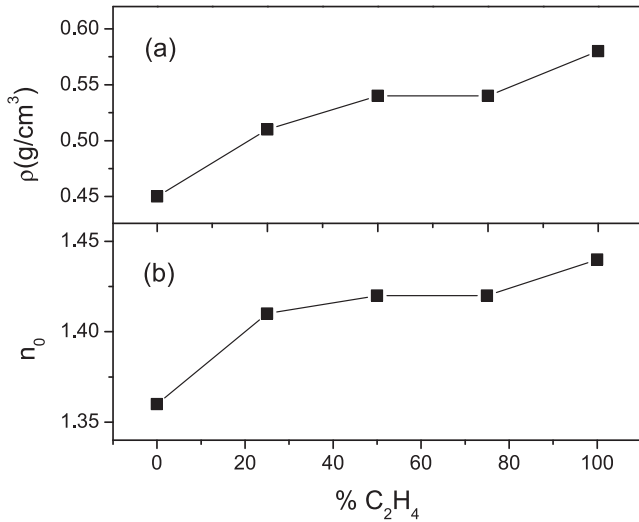


Figure 2. Density (a) and visible refractive index (b) of CH₄:C₂H₄ mixtures at 30 K. The experimental error estimated for these magnitudes is 3 per cent.

Table 1. Numerical values for the density and visible refractive index of CH₄:C₂H₄ mixtures at 30 K.

(CH ₄ :C ₂ H ₄)	ρ (g cm ⁻³)	n ₀
(1:0)	0.45	1.36
(3:1)	0.51	1.41
(1:1)	0.54	1.42
(1:3)	0.54	1.42
(0:1)	0.58	1.44

3 RESULTS

3.1 Density and n₀

Fig. 2 and Table 1 show the results for the density and the visible refractive index of CH₄, C₂H₄ and CH₄:C₂H₄ ice mixtures at 30 K. These magnitudes were already measured in our group for pure CH₄ ice (Satorre et al. 2008; Molpeceres et al. 2016). For the present study we have re-measured the density and obtained 0.45 g cm⁻³, in agreement with Molpeceres et al. (2016) and also, within an experimental error, with Satorre et al. (2008) (0.47 g cm⁻³). The newly determined refractive index also agrees with previously published results. As far as we know, densities of pure ethylene and methane:ethylene ices at 30 K had never been reported. Since growing conditions are known to affect the morphology of the ice sample, different accretion rates were tested, both for CH₄ and C₂H₄, varying between 0.3 and 10 nm s⁻¹. The results for the different rates were found to diverge by less than 3 per cent, which is the estimated experimental error.

The pure species have fairly different refractive indices, 1.36 for CH₄ and 1.44 for C₂H₄. The mixtures present an averaged value, 1.42, that nearly does not change with dilution. Hudson et al. (2014) reported 1.45 for pure crystalline C₂H₄ at 45 K and 1.35 for the metastable phase at 30 K. The value obtained in this work agrees with that of the crystalline phase, and is about 6 per cent higher than that of the metastable phase. Experimental errors and effects due to the different morphologies could explain this discrepancy (see below). As for the visible refractive indices of the mixtures, to our knowledge they are reported here for the first time.

The refractive indices obtained are used for film thickness determination, and as input parameters in the calculations of the optical constants.

We have measured 0.58 g cm⁻³ as the density of pure ethylene ice at 30 K. The only previous data for this magnitude that we could find are by Van Nes & Vos (1979). Those authors conducted X-ray diffraction experiments on monocrystals of ethylene at 85 K, determined the crystal structure of the solid, and derived its density, 0.75 g cm⁻³. Our value of 0.58 g cm⁻³ corresponds to vapour deposited ethylene at 30 K. The discrepancy suggests that our ice, if crystalline, is in a different arrangement from that of the crystalline solid grown by van Nes and coworkers, or that it could have some degree of porosity. It is worth noticing that by slow vapour deposition polycrystalline solid layers, with crystal domains oriented randomly, are formed (Mitling & Leung 2002), in contrast with the pure monocrystal investigated by Van Nes & Vos (1979). At this point, it is important to highlight that the physical conditions of our experiments are closer to astrophysical environments and hence the densities obtained are probably more adequate to simulate astrophysical ices. A similar discrepancy was observed between the density of the low temperature vapour deposited C₂H₆ ice (Molpeceres et al. 2016) and that of the 85 K monocrystal grown (Van Nes & Vos 1978).

The mixtures have densities between those of the pure species. Methane ice grown at 30 K at the deposition rates considered in this work, is in a crystalline (polycrystalline) form. When codeposited with ethylene probably its ordered structure will be destroyed and the resulting structure has larger density. However, in this set of experiments, we have observed that once the fraction of ethylene molecules reach 50 per cent (1:1 mixture), the density remains almost constant for increasing fractions of ethylene. Intermolecular interactions within the solid must play a key role to explain these data. The polarizable methane molecules interact with ethylene molecules via dipole-induced forces. These interactions are affected by the mixing ratio and ultimately are responsible for the different packings and the final density.

The densities given in this section are fundamental magnitudes to understand morphological changes in the ice samples. Moreover, they are crucial for a good estimation of the IR band strengths of the ices that will be presented later in this paper.

3.2 Spectra

Fig. 3 displays the IR spectrum of pure ethylene and Fig. 4 the spectra of the pure species and the 1:1 mixture in the regions of interest. The spectrum of pure ethylene ice can be compared with that of Hudson et al. (2014). These authors prepared different phases of ethylene by modifying the growth conditions, namely deposition rate and temperature. We have worked at 30 K with deposition rates around ~1.4 nm s⁻¹ and have obtained a phase that is between the metastable phase grown by Hudson et al. (2014) at 20 K and 16.7 nm s⁻¹ and the amorphous phase grown by the same authors by slow deposition (1 mm h⁻¹) at 12 K. The three spectra, all recorded at 30 K, are represented in Fig. 3 for comparison. It can be seen that our spectrum resembles the metastable one in the 3000 cm⁻¹ region, while discrepancies are evident in the features at 1434, 945 and 822 cm⁻¹ that present well-resolved double peaks in the metastable phase spectrum and appear weaker and only partially resolved in our spectrum. On the other hand, the ice grown at 30 K in this work looks similar to the amorphous form in this lower frequency range.

By inspecting Fig. 4, it is possible to follow the modifications in the spectra of the mixture with respect to the pure ices. These

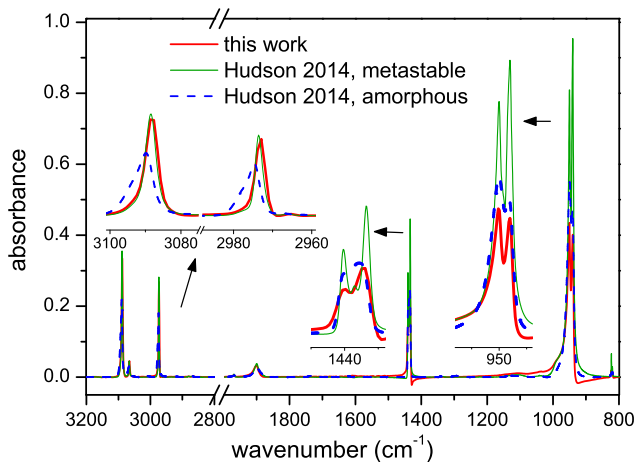


Figure 3. Comparison of IR pure ethylene spectrum obtained in this work with previous literature spectra by Hudson et al. (2014), all at 30 K. The literature spectra correspond to ices 0.931 μm thick (metastable) and 2.85 μm thick (amorphous) and have been multiplied by 1.5 and 0.49 to compare with the 1.4- μm -thick spectrum obtained in this work.

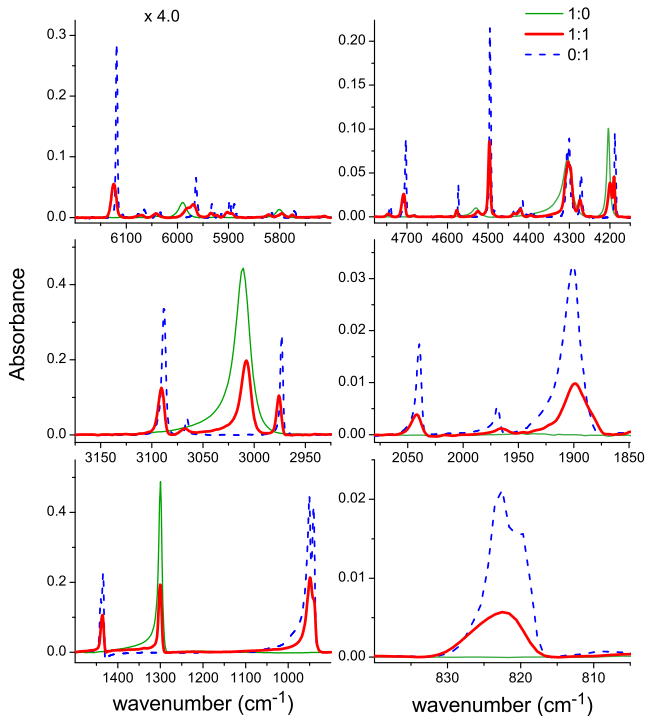


Figure 4. IR spectra of pure CH_4 (1:0, green, thin line), pure C_2H_4 (0:1, blue, dashed line) and a 50 per cent number molecule mixture (red, thick line) ices deposited at 30 K. Ice thickness is 6.5 μm in the top panels (NIR) and 1.4 μm in the others (MIR). Files of the spectra presented in the figure are given in the supplementary material.

modifications consist of frequency shifts, band broadening, and in some cases changes in band profile. For example, the doublets in the spectra of pure ethylene at 1434 and 945 cm^{-1} are blended in the spectrum of the 1:1 mixture. Fig. 5 displays the spectra of the three mixtures investigated, and the evolution of the different absorption peaks with the mixing ratio is well appreciated. If we look again at the 945 cm^{-1} ethylene band, its band-width is larger in the 3:1 than in the 1:3 ($CH_4:C_2H_4$) mixture. Similar band broadening with dilution are observed for other bands. This behaviour can be

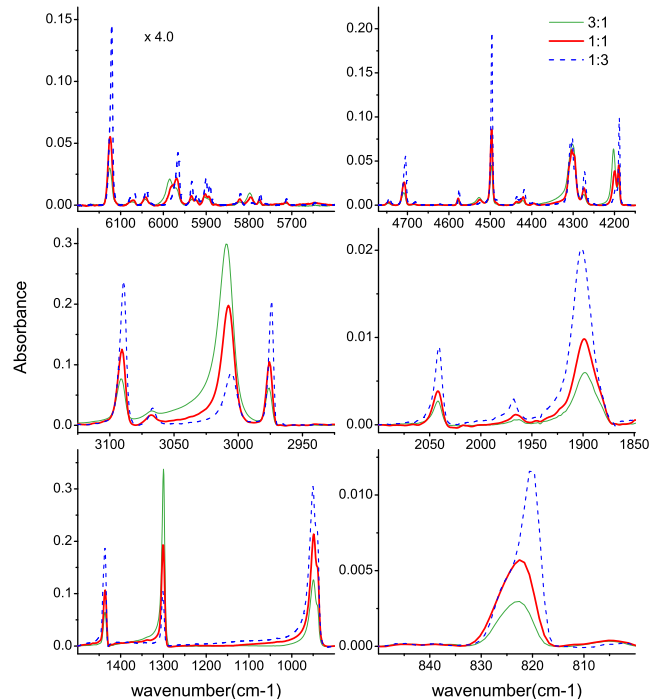


Figure 5. IR spectra of $CH_4:C_2H_4$ ice mixtures at 30 K with different composition ratio (3:1, green, thin line, 1:1, red, thick line, and 1:3 blue, dashed line). Ice thickness is 6.5 μm in top panels (NIR) and 1.4 μm in the others (MIR). Files of the spectra presented in the figure are given in the supplementary material.

interpreted as if the amorphous character of each particular species increases with its dilution in the mixture, a fact that is corroborated by the appearance of a very weak, not appreciable in Fig. 4, ν_1 band of CH_4 , forbidden by symmetry in the pure crystalline CH_4 ice.

3.2.1 Band shifts

We have quantified the frequency shifts of methane or ethylene bands in the mixtures investigated. The band shifts are defined as $\nu_{\text{mixture}} - \nu_{\text{pure}}$. Fig. 6 shows the measured band shifts versus mixture ratio for several bands of methane and ethylene in the NIR region. It can be seen that methane bands shift to lower frequency when diluted in ethylene (top panel) while ethylene bands shift to higher frequency when diluted in methane (lower panel). Band shifts of methane in ice mixtures were addressed in the bibliography in mixtures with nitrogen or water (Hudgins et al. 1993; Quirico & Schmitt 1997; Gálvez et al. 2009) showing a displacement to lower wavenumbers when diluted in nitrogen and to lower or higher wavenumbers depending on its dilution in water. In contrast, ethylene IR bands in ice mixtures with nitrogen suffer a clear displacement to higher wavenumbers (Quirico & Schmitt 1997). Therefore, it can be said that non-polar or low-polar environments tend to displace methane vibrations to lower wavenumbers and ethylene vibrational frequencies to higher values. Concerning the evolution of the band shifts with mixture ratio, the behaviour is also different for the two species. The more diluted the methane, the larger the shift. For ethylene, the higher shifts occur at high ethane concentration and then the shift decreases with increasing dilution.

3.2.2 Band strengths

We have determined integrated band strengths of the main methane and ethane absorptions in the NIR and MIR regions in the ice

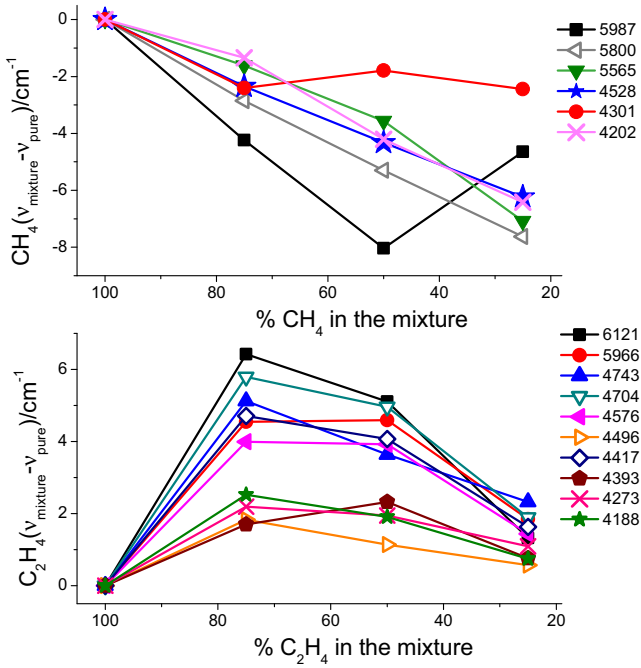


Figure 6. Methane (upper panel) and ethylene (bottom panel) band shifts for several NIR absorptions in binary mixtures. The band centres (in cm^{-1}) for the various bands of CH_4 and C_2H_4 are listed in the upper and lower panels, respectively. Files with all the band shifts measured in this work are provided in the supplementary material.

mixtures investigated, and have compared them to the corresponding values for pure species. In order to calculate these magnitudes two different procedures are usually followed. In the first one, the apparent band strengths (denoted as A' following the notation by Hudson et al. 2014) are extracted by direct integration of the bands in the absorbance spectra, defining an adequate baseline in each case, using

$$A' = \frac{2.303}{\rho_N L} \int_{\text{band}} A(\bar{\nu}) d\bar{\nu}. \quad (1)$$

The molecular density (ρ_N) of a particular absorber in the mixture and the ice layer thickness (L) must be known. Although this method is broadly employed in the literature to obtain band strengths, the derived magnitudes may be affected by possible intensity losses or interference effects present in the spectra of thin films due to IR reflections in the different interfaces.

In the second procedure, absolute band strengths (denoted as A , again following Hudson et al. 2014) free from those undesired effects, can be obtained if the imaginary component of the refractive index, $k(\bar{\nu})$, is known, by means of

$$A = \frac{4\pi}{\rho_N} \int_{\text{band}} \bar{\nu} k(\bar{\nu}) d\bar{\nu}. \quad (2)$$

The procedure employed in this work to derive the optical constants from a set of ice layers of different thickness is described in Section 3.3.

Densities have been taken from Table 1. They have to be converted to molecular densities for each particular component in the mixtures, in order to include them in equation (1) or (2). The conversion was made from the molecular weights and mixing ratios of each component, with the results shown in Table 2. Band strengths thus calculated are presented in Tables 3 and 4 for CH_4 and C_2H_4 ices,

Table 2. Molecular densities ($\times 10^{22}$ molecules cm^{-3}) of each species in the mixtures investigated in this work.

Mixture ratio ($\text{CH}_4:\text{C}_2\text{H}_4$)	ρ_N (tot)	ρ_N (CH_4)	ρ_N (C_2H_4)
1:0	1.69	1.69	–
3:1	1.61	1.21	0.40
1:1	1.47	0.74	0.74
1:3	1.30	0.33	0.98
0:1	1.25	–	1.25

respectively. The $k(\bar{\nu})$ values needed for equation (2) are given in Section 3.3.

The long dashes in Tables 3 and 4 correspond to blended absorptions for which it was not possible to separate methane and ethylene contributions, and no integration was performed. It can be seen that both A and A' provide similar results differing by less than 30 per cent. Our estimated experimental uncertainty is of the same order. The experimental error arises mainly from the integration process, where choices for baseline and band limits are particularly complicated in these mixtures where the bands of CH_4 and C_2H_4 appear very close and sometimes even overlap. Other sources of error lie in the determination of ice thickness, estimated to be less than 5 per cent, and stoichiometry, also estimated to be well below 5 per cent, owing to the good reproducibility and stability provided by the mass flow controllers.

Inspecting Table 3 it is possible to recognize a general intensity trend for the methane bands with dilution. In general terms, a weakening is observed with increasing dilution. A similar tendency was observed for methane in $\text{CH}_4:\text{C}_2\text{H}_6$ (Molpeceres et al. 2016) or $\text{CH}_4:\text{H}_2\text{O}$ (Bossa et al. 2015) ice mixtures. An opposite behaviour has also been observed when the dilution of methane is much higher, up to 20:1, in a wide variety of molecules such as CO , CO_2 , N_2 (Hudgins et al. 1993). All these studies indicate that the band strengths of methane vibrations in the ice are strongly dependent on the kind of intermolecular interactions between methane and its counterpart, but also on the degree of dilution. In this way, both factors must be taken into account in order to extract any conclusion.

The ethylene band strengths, much less studied than those of methane, do not show a preferential trend (see Table 4). Each band behaves differently. For the most intense IR absorption at 945 cm^{-1} , little variations of the band strength are observed with dilution. In contrast, a quite strong absorption at 2973 cm^{-1} shows a remarkable intensity increase with dilution, which suggests a strong interaction and intensity sharing with vibrations of nearby methane molecules. In general, we are not able to predict the trend of a certain vibration with respect to dilution, due to the complexity of the interactions in the mixture.

3.3 Optical constants

Other interesting magnitudes determined in this work are the IR optical constants for pure ethylene ice and for the three mixtures investigated. To derive these magnitudes a set of IR spectra for each particular ice has been obtained as a function of thickness. In the MIR spectral range, to avoid saturation of the stronger absorptions, ice layers up to $\sim 1.5 \mu\text{m}$ were grown. In the NIR spectral region, in order to have good signal to noise ratio for the weak absorptions that the ices present in this region, ice layers up to $6 \mu\text{m}$ were generated.

Table 3. Band strengths ($\times 10^{-18}$ cm per molecule) A and A' of selected absorption features of CH_4 in the pure ice and in the mixtures obtained using the imaginary component of the complex refractive index, or the integrated absorbance spectrum, respectively.

Peak position		(1:0)		(3:1)		(1:1)		(1:3)	
cm^{-1}	μm	A	A'	A	A'	A	A'	A	A'
5987	1.670	0.027	0.026	–	–	–	–	–	–
5800	1.724	0.015	0.015	0.011	0.018	0.018	0.010	0.004	0.011
5565	1.797	0.008	0.006	0.005	0.007	0.007	0.005	–	0.002
4528	2.208	0.052	0.060	0.026	0.029	0.029	0.025	0.011	0.018
4301	2.325	0.496	0.478	–	–	–	–	–	–
4202	2.380	0.252	0.237	0.117	0.136	0.136	0.086	0.031	0.047
3010	3.322	10.402	10.835	6.593	7.156	5.621	6.590	4.501	5.793
1300	7.692	6.905	8.029	5.404	6.310	4.699	5.025	3.786	5.200

Table 4. Band strengths ($\times 10^{-18}$ cm per molecule) A and A' of selected absorption features of C_2H_4 in the pure ice and in the mixtures obtained using the imaginary component of the complex refractive index, or the integrated absorbance spectrum, respectively.

Peak position		(3:1)		(1:1)		(1:3)		(0:1)	
cm^{-1}	μm	A	A'	A	A'	A	A'	A	A'
6121	1.634	0.089	0.077	0.083	0.086	0.113	0.111	0.087	0.091
5966	1.676	–	–	–	–	–	–	0.027	0.027
4743	2.108	0.023	0.020	0.021	0.020	0.027	0.023	0.020	0.018
4704	2.126	0.140	0.122	0.133	0.137	0.180	0.176	0.138	0.149
4576	2.185	0.027	0.024	0.026	0.025	0.035	0.034	0.028	0.030
4496	2.224	0.304	0.264	0.299	0.305	0.408	0.402	0.321	0.340
4417	2.264	0.072	0.063	0.069	0.030	0.091	0.042	0.070	0.076
4393	2.276	0.009	0.008	0.008	0.010	0.012	0.011	0.010	0.009
4306	2.322	–	–	–	–	–	–	0.295	0.319
4273	2.340	0.050	0.044	0.067	0.071	0.107	0.107	0.090	0.097
4188	2.388	0.055	0.048	0.065	0.076	0.124	0.130	0.127	0.137
3088	3.238	2.675	2.586	2.467	2.395	2.601	2.898	2.395	2.623
3065	3.263	0.284	0.275	0.324	0.308	0.297	0.340	0.269	0.269
2973	3.364	1.732	1.675	1.514	1.375	1.590	1.682	1.228	1.375
2039	4.904	0.157	0.152	0.130	0.119	0.144	0.143	0.149	0.170
1901	5.260	0.882	0.853	0.686	0.593	0.890	0.877	0.816	1.021
1434	6.974	3.082	2.979	2.700	2.988	3.057	3.774	2.930	4.211
945	10.582	17.918	17.321	16.430	13.091	17.137	15.563	15.896	16.504
822	12.165	0.134	0.129	0.140	0.095	0.137	0.125	0.172	0.170

The procedure to calculate the optical constants varies depending on the spectral region considered, as described in previous works (Zanchet et al. 2013; Molpeceres et al. 2016). The software, developed in our group, is available online in our web page (<http://www.iem.csic.es/fismol/fmap/descarga.htm>). An iterative method is implemented in the MIR with an algorithm described in detail by Zanchet et al. (2013). Briefly, two multidimensional functions, defined as differences between experimental and calculated spectra, are minimized iteratively. To calculate the transmission spectra through a three-layer system like our experimental one, an analytical model based on Fresnel coefficients was employed. Several variables are fitted: k and n at each wavelength, ice thickness, visible refractive index, and the ratio of coherent/incoherent transmitted IR radiation. To carry out this fitting, several experimental spectra of different thickness are necessary, as well as accurate measurements of the film thickness and of the refractive index n_0 of the ice. After the iterative procedure, the final fitted thickness and visible refractive indices differ from the measured values by less than the experimental error. This condition is used as a measure of the consistency of the fitting.

For the NIR region, this procedure cannot be used due to problems in the baseline simulation, which is affected by scattering and double IR reflections. These effects are of the same order of magnitude than the NIR absorptions. Hence, in this frequency range, after a proper subtraction of a baseline in the absorbance spectrum, Lambert's law is applied to obtain the imaginary part of the refractive index:

$$k(\bar{\nu}) = 2.303 \frac{1}{4\pi\bar{\nu}L} A(\bar{\nu}), \quad (3)$$

where L is the ice thickness, $A(\bar{\nu})$ the absorbance spectrum and $k(\bar{\nu})$ the imaginary part of the refractive index. The real part of the refractive index is subsequently obtained using the Kramers–Kronig relation. Optical constants of the mixtures are presented in Fig. 6. The corresponding n_0 values are the ones given in Table 1. Optical constants for the mixtures are presented in Fig. 7.

We have calculated also the optical constants of pure ethylene ice at 30 K. Fig. 8 shows a comparison of absorption coefficients, $\alpha(\bar{\nu}) = 4\pi\bar{\nu}k(\bar{\nu})$ in the NIR and $k(\bar{\nu})$ values in the MIR obtained from the present data with previous results. Although the

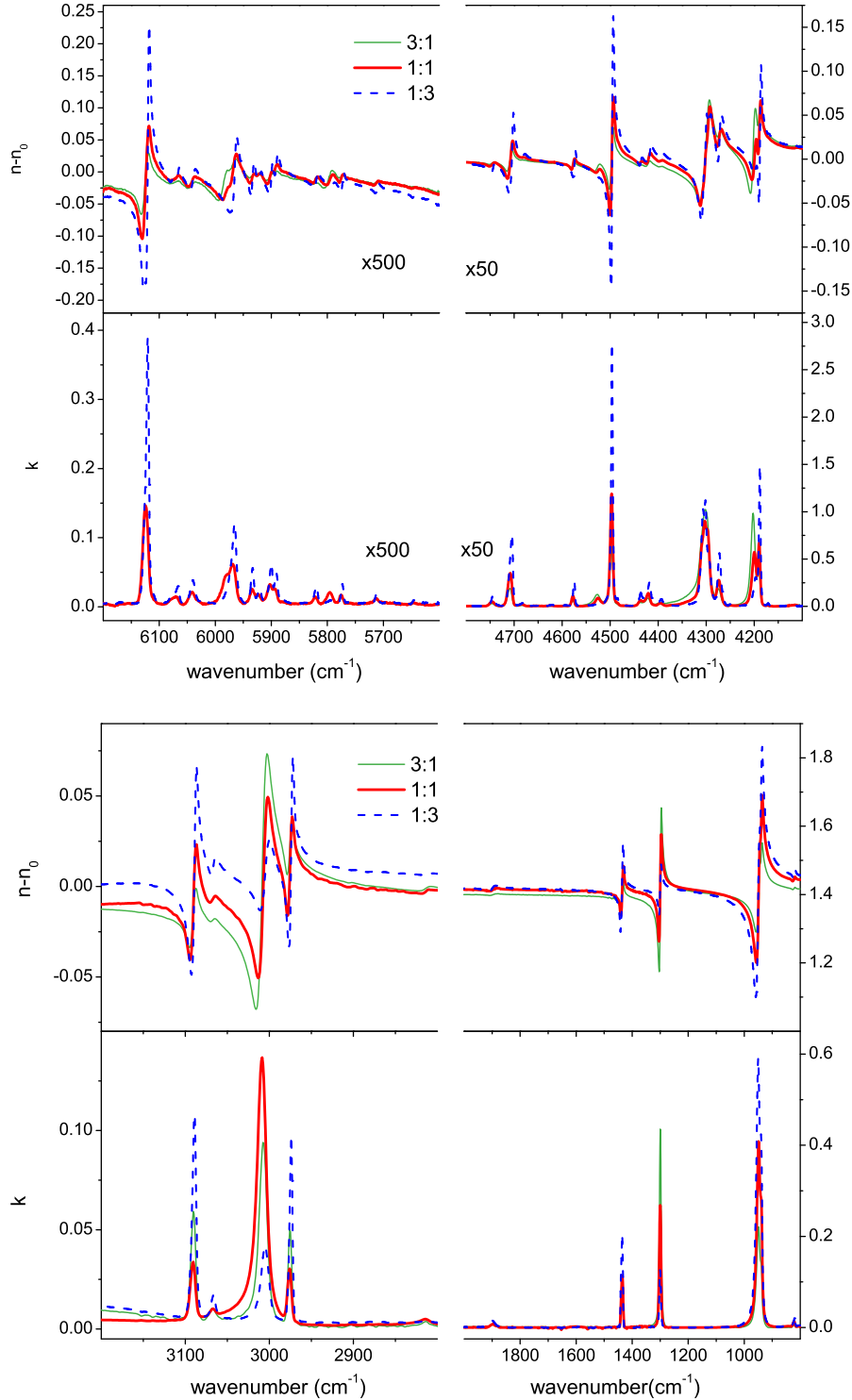


Figure 7. Optical constants in the more relevant NIR and MIR spectral regions of $\text{CH}_4:\text{C}_2\text{H}_4$ ices with proportions (3:1), (1:1) and (1:3) at 30 K. Files with the optical constants determined in this work for pure species and mixtures are given in the supplementary material.

absorption coefficients given by Quirico & Schmitt (1997) and those of Hudson et al. (2014) do not correspond exactly to the same phase of ethylene ice, the agreement in the NIR region is quite good (Fig. 8, top panel). The comparison of $k(\bar{\nu})$ in the MIR region with the data of Hudson et al. (2014) manifests the different phases of the ices that were already commented on in Fig. 3 (Fig. 8, bottom panel).

3.4 Astrophysical implications

In the last two decades methane has been detected in many objects of our Solar system (Mars, satellites as Titan or Triton, and TNOs as Pluto, Eris, Sedna or Makemake). During this period, many laboratories devoted to the study of ices and their evolution under irradiation, have determined the formation of complex

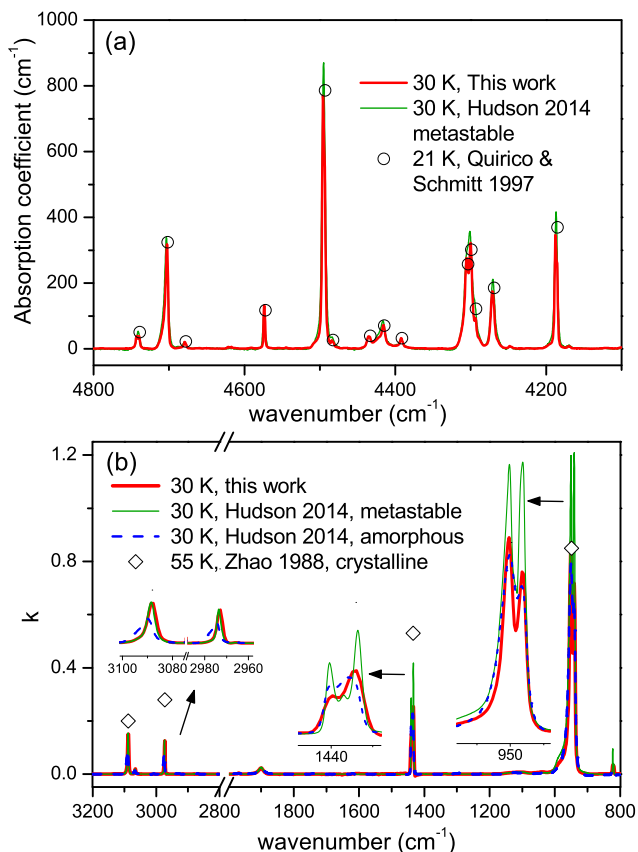


Figure 8. Absorption coefficients (a) and imaginary part of the refractive index (b) of pure ethylene ice at 30 K determined in this work compared with previous literature data.

molecules derived from it. The final products depend on the dose and also on the surface refreshing time. The higher the irradiation dose is, the larger (less hydrogenated) molecules are formed. Also when the dose increases, a quasi-equilibrium is established between molecular formation and destruction until a plateau in abundance is attained. The faster the methane is renewed, the lighter the products of irradiation will be, since simple products such as ethane or ethylene cannot evolve to larger ones as new CH_4 covers them. Very different products are formed after irradiation of methane ice mixtures. For example, when methane is diluted in N_2 , which is relevant for objects like Triton or Pluto (Cruikshank et al. 1993; Stern et al. 2015), the new species formed will contain nitrogen and carbon atoms (i.e. Hudson & Moore 2002).

In order to apply our results in an astrophysical context, the total dose of surface irradiation of the object along time, but also how CH_4 is renewed on it (refreshing time), must be taken into account. The renewal mechanisms could involve differential buoyancy with respect to the dominant molecule (Luna et al. 2012; Roe & Grundy 2012), as seems to be the case for Triton, or differential sublimation that segregates methane with respect to other volatiles such as nitrogen (Douté et al. 1999; Licandro et al. 2006; Merlin et al. 2009) or, even cryovolcanism (Kargel 1994).

We can focus our attention on the dwarf planet Makemake to stress the usefulness of our results on $CH_4:C_2H_4$ mixtures for investigations of this object, and why they can be applied for other objects of similar composition and evolution. Makemake seems to have been originally covered by nitrogen, but in contrast to more massive objects like Pluto, Triton or Eris, Makemake was not able

to retain nitrogen due to its low gravity (Brown, Schaller & Blake 2015). Initially only CH_4 was detected on the surface of Makemake (Barucci et al. 2008); after that, ethane was confirmed (Brown et al. 2007), and finally, ethylene, acetylene and probably propane (Brown et al. 2015) have been found, as a result of specific searches. Among these molecules, C_2H_6 and C_3H_8 are the more and less abundant, respectively. These observations suggest a renewal mechanism for its surface, probably due to seasonal temperature changes along Makemake’s orbit (309 Earth years). The fact that new material refreshes the surface of Makemake does not exclude the possibility that part of the carbon chains become larger and dehydrogenated, forming tholins.

By analogy with the evolution occurred on Makemake’s surface, probably other objects will present ethylene signatures when future instrumentation, as NIRSPEC on the *James Webb Space Telescope*, will become available. As a matter of fact C_2H_x products have been detected on Pluto’s atmosphere by the *New Horizons* mission (Stern et al. 2015), probably coming from pure methane irradiated on its surface, although part of them could be formed in Pluto’s haze (Gladstone et al. 2016). With increasing observational resolution and sensitivity, the details in the observed NIR methane spectrum could probably be explained in terms of not only dilution in N_2 , but also as due to ethane (Molpeceres et al. 2016) or ethylene diluted on methane (this work). With all these considerations the results presented in this paper provide tools for a better understanding of the composition of the icy surface of different objects such as Makemake, Pluto or Eris.

4 SUMMARY AND CONCLUSIONS

(1) In this work, we have investigated pure ethylene and methane:ethylene ice mixtures at 30 K. In one set of experiments, we have determined densities and visible refractive indices by means of a cryogenic quartz crystal microbalance and He–Ne laser interferometric techniques. In another one, we have measured spectroscopically relevant magnitudes such as band shifts, band strengths and IR optical constants in the NIR and MIR spectral regions.

(2) The densities of these materials range from 0.45 g cm^{-3} for pure methane ice to 0.58 g cm^{-3} for pure ethylene. We have re-measured the density of methane and confirmed the previous value of Satorre et al. (2008). Our ices are grown by vapour deposition under vacuum, a procedure that is supposed to better mimic the structure of astrophysical ices. We did not find any previous data for ethylene using this method.

(3) We have measured wavenumber shifts in the spectra of mixed species with respect to those of the pure compounds. These deviations are useful to identify the presence of methane or ethylene and their particular environments from observations. The degree of dilution of the particular species in the ice mixture affects the peak displacements, which can change from positive to negative with respect to the pure species. In particular, it should be stressed that ethylene bands undergo a larger displacement when there is a small methane fraction in the $CH_4:C_2H_4$ mixtures than when methane is dominant.

(4) We report IR band strengths for pure ethylene and for mixtures. For methane bands in the mixtures, an overall decrease of band strengths with respect to the pure species is observed. For ethylene no particular trend is found, the behaviour depending on the band under consideration.

(5) We have also calculated optical constants in the NIR and the MIR spectral regions for the three mixtures and for pure ethylene.

These optical constants are expected to be useful for modeling astronomical environments.

ACKNOWLEDGEMENTS

This work has been funded by the Ministerio de Ciencia y Competitividad (MINECO) of Spain under grants FIS2013-48087-C2-1P, FIS2013-48087-C2-2P and AYA2015-71975-REDT ‘Polvo Cósmico’ by the Ministerio de Ciencia e Innovación of Spain under grant CDS2009-00038 and by the European Research Council project ERC-2013-Syg 610256 ‘Nanocosmos’. GM acknowledges MINECO PhD grant BES-2014-069355. Our skillful technicians C. Santonja, M. A. Moreno, A. González and J. Rodríguez are also gratefully acknowledged.

REFERENCES

- Barucci M. A., Dalle Ore C. M., Alvarez-Candal A., de Bergh C., Merlin F., Dumas C., Cruikshank D., 2010, *AJ*, 140, 2095
- Barucci M. A. et al., 2008, *A&A*, 479, L13
- Bossa J.-B., Maté B., Fransen C., Cazaux S., Pilling S., Rocha W. R. M., Ortigoso J., Linnartz H., 2015, *ApJ*, 814, 47
- Brown M. E., Barkume K. M., Blake G. A., Schaller E. L., Rabinowitz D. L., Roe H. G., Trujillo C. A., 2007, *AJ*, 133, 284
- Brown M. E., Schaller E. L., Blake G. A., 2015, *AJ*, 149, 105
- Chen H.-F., Liu M.-C., Chen S.-C., Huang T.-P., Wu Y.-J., 2015, *ApJ*, 804, 36
- Cruikshank D. P. et al., 2015, *Icarus*, 246, 82
- Cruikshank D. P., Roush T. L., Owen T. C., Geballe T. R., de Bergh C., Schmitt B., Brown R. H., Bartholomew M. J., 1993, *Science*, 261, 742
- DeMeo F. E. et al., 2010, *Icarus*, 208, 412
- de Vries A. E., Pedrys R., Haring R. A., Haring A., Saris F. W., 1984, *Nature*, 311, 39
- Douté S., Schmitt B., Quirico E., Owen T. C., Cruikshank D. P., de Bergh C., Geballe T. R., Roush T. L., 1999, *Icarus*, 142, 421
- Gálvez Ó., Maté B., Herrero V. J., Escribano R., 2009, *ApJ*, 703, 2101
- Gerakines P. A., Hudson R. L., 2015, *ApJ*, 805, L20 (5pp).
- Gladstone G. R. et al., 2016, *Science*, 80, 351
- Hudgins D. M., Sandford S. A., Allamandola L. J., Tielens A. G., 1993, *ApJS*, 86, 713
- Hudson R. L., Moore M. H., 2002, *ApJ*, 568, 1095
- Hudson R. L., Gerakines P. A., Moore M. H., 2014, *Icarus*, 243, 148
- Kaiser R. I., Roessler K., 1992, *Ann. Geophys.*, 10, 222
- Kargel J. S., 1994, *Earth Moon Planets*, 67, 101
- Licandro J., Grundy W. M., Pinilla-Alonso N., Leisy P., 2006, *A&A*, 458, L5
- Luna R., Satorre M. Á., Domingo M., Millán C., Santonja C., 2012, *Icarus*, 221, 186
- Merlin F., 2015, *A&A*, 582, A39
- Merlin F. et al., 2009, *AJ*, 137, 315
- Mitling S., Leung K. T., 2002, *J. Phys. Chem. B*, 106, 6234
- Mulas G., Baratta G. A., Palumbo M. E., Strazzulla G., 1998, *A&A*, 333, 1025
- Molpeceres G., Satorre M. Á., Ortigoso J., Millán C., Escribano R., Maté B., 2016, *ApJ*, 825, 156
- Quirico E., Schmitt B., 1997, *Icarus*, 127, 354
- Roe H. G., Grundy W. M., 2012, *Icarus*, 219, 733
- Satorre M. Á., Leliwa-Kopystynski J., Santonja C., Luna R., 2013, *Icarus*, 225, 703
- Satorre M. Á., Domingo M., Millán C., Luna R., Vilaplana R., Santonja C., 2008, *Planet. Space Sci.*, 56, 1748
- Stern S. A. et al., 2015, *Science*, 80, 350
- Strazzulla G., Baratta G., Domingo M., Satorre M. Á., 2002, *Nucl. Instrum. Methods B*, 191, 714
- Van Nes G. J. H., Vos A., 1979, *Acta Cryst.*, 35, 2593
- Van Nes G. J. H., Vos A., 1978, *Acta Cryst.*, 34, 1947
- Zanchet A., Rodríguez-Lazcano Y., Gálvez Ó., Herrero V. J., Escribano R., Maté B., 2013, *ApJ*, 777, 26
- Zhao G., Ospina M. J., Khanna R. K., 1988, *Spectrochim. Acta*, 44A, 27

SUPPORTING INFORMATION

Supplementary data are available at [MNRAS](#) online.

Supplementary material.7z

Please note: Oxford University Press is not responsible for the content or functionality of any supporting materials supplied by the authors. Any queries (other than missing material) should be directed to the corresponding author for the article.

This paper has been typeset from a $\text{\TeX}/\text{\LaTeX}$ file prepared by the author.